Computation of vertically averaged velocities in irregular sections of straight channels

ELEONORA SPADA, PhDstudent, *Dipartimento di Ingegneria Civile, Ambientale,Aerospaziale, dei Materiali (DICAM),Università degli studi di Palermo, Viale delle scienze, 90128, Palermo, Italy.*

Email: eleonora.spada@unipa.it (author for correspondence)

TULLIO TUCCIARELLI , Professor, *Dipartimento di Ingegneria Civile, Ambientale,Aerospaziale, dei Materiali (DICAM),Università degli studi di Palermo, Viale delle scienze, 90128, Palermo, Italy.*

Email: tullio.tucciarelli@unipa.it

MARCO SINAGRA , PhD, *Dipartimento di Ingegneria Civile, Ambientale,Aerospaziale, dei Materiali (DICAM),Università degli studi di Palermo, Viale delle scienze, 90128, Palermo, Italy.*

VINCENZO SAMMARTANO, PhD, *Dipartimento di Ingegneria Civile, dell'Energia, dell'Ambiente e dei Materiali (DICEAM), Università Mediterranea di Reggio Calabria, Via Graziella, 89122, Reggio Calabria, Italy.*

GIOVANNI CORATO, Researcher, Centre de Recherche Public 'Gabriel Lippmann',41 rue du Brill, L-4422 Belvaux, Luxembourg.

Computation of vertically averaged velocities in irregular sections of straight channels

ABSTRACT

Two new methods for vertically averaged velocity computation are presented, validated and compared with other available formulas. The first method derives from the well-known Huthoff algorithm, which is first shown to be dependent on the way the river cross-section is discretized into several sub-sections. The second method assumes the vertically averaged longitudinal velocity to be a function only of the friction factor and of the so-called "local hydraulic radius", computed as the ratio between the integral of the elementary areas around a given vertical and the integral of the elementary solid boundaries around the same vertical. Both integrals are weighted with a linear shape function, equal to zero at a distance from the integration variable which is proportional to the water depth according to an empirical coefficient β. Both formulas are validated against 1) laboratory experimental data, 2) discharge hydrographs measured in a real site, where the friction factor is estimated from an unsteady-state analysis of water levels recorded in two different river cross sections, 3) the 3D solution obtained using the commercial ANSYS CFX code, computing the steady state uniform flow in a cross section of the Alzette river.

Keywords: diffusive model,discharge estimation, irregular section, rating curve, uniform flow.

1 Introduction

Computation of vertically averaged velocities is the first step of two major calculations in 1D shallow water modelling: 1) estimation of the discharge given the energy slope and the water stage and 2) estimation of the bottom shear stress for computing the bed load in a given river section.

Many popular software tools, like MIKE11 (MIKE11, 2009), compute the discharge Q, in each river section, as the sum of discharges computed in different sub-sections, assuming a single water stage for all of them. Similarly, HEC-RAS (HEC-RAS,2010) calculates the conveyance of the cross-section by the following form of Manning's equation:

$$Q = KS_f^{1/2} \quad (1),$$

where S_f is the energy slope and K is the conveyance, computed assuming the same hypothesis and solving each sub-section according to the traditional Manning equation.

The uniform flow formula almost universally applied in each sub-section is still the Chezy equation (Herschel, C., 1897). The advantage of using the Chezy equation is that the associated Manning's coefficient has been calibrated worldwide for several types of bed surface and a single value is ready to use for each application. However, it is well known that the Chezy equation was derived from laboratory measurements taken in channels with a regular, convex cross-sectional shape. When the section results from the union of different parts, each with a strongly different average water depth, one of two options is usually selected. The first option, called Single Channel Method (SCM) is simply to ignore the problem. This leads to strong underestimation of the discharge, because the Chezy formula assumes a homogeneous vertically averaged velocity and this homogeneous value provides strong energy dissipation in the parts of the section with lower water depths. The second option, called Divided Channel Method (*DCM*) is to compute the total discharge as the sum of the discharges flowing in each convex part of the section (called subsection) , assuming a single water level for all parts (Chow 1959; Shiono et al. 1999; Myers and Brennan, 1990). In this approach, the wet perimeter of each subsection is restricted to the component of the original one pertaining to the subsection, but the new components shared by each couple of subsections are neglected. This is equivalent to neglecting the shear stresses coming from the vortices with vertical axes (if subsections are divided by

vertical lines) and considering additional resistance for higher velocities, which results in overestimation of discharge capacity (Lyness et al. 2001).

Knight and Hamed (1984) compared the accuracy of several subdivision methods for compound straight channels by including or excluding the vertical division line in the computation of the wetted perimeters of the main channel and the floodplains. However, their results show that conventional calculation methods result in larger errors. Wormleaton et al. (1982) and Wormleaton and Hadjipanos(1985) also discussed, in the case of compound sections, the horizontal division through the junction point between the main channel and the floodplains. Their studies show that these subdivision methods cannot well assess the discharge in compound channels.

The interaction phenomenon in compound channels has also extensively studied by many other researchers (e.g., Sellin 1964; Knight and Demetriou 1983; Stephenson and Kolovopoulos 1990; Rhodes and Knight 1994; Bousmar and Zech 1999; van Prooijen et al. 2005; Moreta and Martin-Vide 2010). These studies demonstrate that there is a large velocity difference between the main channel and the floodplain, especially at low relative depth, leading to a significant lateral momentum transfer. The studies by Knight and Hamed(1984), Wormleaton et al. (1982) indicate that vertical transfer of momentum between the upper and the lower main channels exists, causing significant horizontal shear able to dissipate a large part of the flow energy.

Furthermore, many authors have tried to quantify flow interaction among the subsections, at least in the case of compound, but regular channels. To this end turbulent stress was modelled through the Reynolds equations and coupled with the continuity equation (Shiono and Knight, 1991). This coupling leads to equations that can be analytically solved only under the assumption of negligible secondary flows. Approximated solutions can also be obtained, although they are based on some empirical parameters. Shiono and Knight developed the Shiono-Knight Method (*SKM*) for prediction of lateral distribution of depth-averaged velocities and boundary shear stress in prismatic compound channels (Shiono and Knight, 1991; Knight and Shiono, 1996). The method can deal with all channel shapes that can be discretized into linear elements (Knight and Abril, 1996; Abril and Knight, 2004).

Other studies based on the Shiono and Knight method can be found in Liao and Knight (2007), Rameshwaran and Sjiono (2007), Tang and Knight (2008) and Omran and Knight (2010). Apart from *SKM*, some other methods for analysing the conveyance capacity of compound channels have been proposed. For example,

117 Ackers (1993) formulated the so called empirical coherence method. Lambert and
118 Sellin(1996) suggested a mixing length approach at the interface, whereas more
119 recently Cao et al. (2006) reformulated flow resistance through lateral integration
120 using a simple and rational function of depth-averaged velocity. Bousmar and Zech
121 (1999) considered the main channel/floodplain momentum transfer proportional to the
122 product of the velocity gradient at the interface times the mass discharge exchanged
123 through this interface due to turbulence. This method, called *EDM*, also requires a
124 geometrical exchange correction factor and turbulent exchange model coefficient for
125 evaluating discharge.
126 A simplified version of the *EDM*, called Interactive Divided Channel Method
127 (*IDCM*), was proposed by Huthoff et al. (2008). In *IDCM* lateral momentum is
128 considered negligible and turbulent stress at the interface is assumed to be
129 proportional to the span wise kinetic energy gradient through a dimensionless
130 empirical parameter α. *IDCM* has the strong advantage of using only two parameters,
131 α and the friction factor, *f*. Nevertheless, as shown in the next section, α depends on
132 the way the original section is divided.
133 An alternative approach could be to simulate the flow structure in its complexity by
134 using a three-dimensional code for computational fluid dynamics (CFD). In these
135 codes flow is represented both in terms of transport motion (mean flow) and
136 turbulence by solving the Reynolds Averaged Navier Stokes (RANS) equations
137 (Wilcox, 2006) coupled with turbulence models. These models allow closure of the
138 mathematical problem by adding a certain number of additional partial differential
139 transport equations equal to the order of the model. In the field of the simulation of
140 industrial and environmental laws second order models (e.g. k-ε and k-ω models) are
141 widely used. Nonetheless, CFD codes need a mesh fine enough to solve the boundary
142 layer (Wilcox, 2006), resulting in a computational cost that can be prohibitive even
143 for river of few km.
144 In this study two new methods, aimed to represent subsection interactions in a
145 compound channel, are presented. The first method, named "INtegrated Channel
146 Method" (*INCM*), derives from the previous Huthoff formula, which is shown to give
147 results depending on the way the river cross section is discretized in sub-sections. The
148 same dynamic balance adopted by Huthoff is written in differential form, but its

diffusive term is weighted according to a ξ coefficient proportional to the local water depth.

The second one, named “local hydraulic radius method” (*LHRM*), derives from the observation that, in the Manning formula, the mean velocity per unit energy gradient is proportional to a power of the hydraulic radius. It should then be possible to get the vertically averaged velocity along each vertical by using the same Manning formula, where the original hydraulic radius is changed with a "local" one. This "local" hydraulic radius should take into account the effect of the surrounding section geometry, up to a maximum distance which is likely to be proportional to the local water depth, according to an empirical β coefficient. The method gives up the idea of solving the Reynolds equations, due to the uncertainty of its parameters, but relies on the solid grounds of the historical experience of the Manning equation.

The present paper is organized as follows: Two of the most popular approaches adopted for computation of the vertically averaged velocities are explained in details, along with the proposed *INCM* and *LHRM* methods. The ξ and β parameters of respectively the *INCM* and *LHRM* methods are then calibrated from available discharge lab experimental data and a sensitivity analysis is carried out. The *INCM* and *LHRM* methods are finally validated according to three different criteria. The first criterion is comparison with other series of the previous laboratory data, not used for calibration. The second criterion is comparison with discharge data measured in one section of the Alzette river Basin (Luxembourg). Because the friction factor is not known a priori, *INCM* and *LHRM* formulas are applied in the context of the indirect discharge estimation method, which simultaneously estimates the friction factor and the discharge hydrograph from the unsteady state water level analysis of two water level hydrographs measured in two different river sections. The third validation criterion is comparison with the vertical velocity profiles obtained by the ANSYS CFX solver, in a cross section of the Alzette river. In the conclusions, it is finally shown that application of bed load formulas, carried out by integration of elementary solid fluxes computed as function of the vertically averaged velocities, can lead to results that are strongly different from those obtained by using the simple mean velocity and water depth section values.

2 Divided Channel Method (*DCM*) and Interactive Divided Channel Method (*IDCM*)

In the *DCM* method the river section is divided into subsections with uniform velocities and roughness (Chow, 1959). Division is made by vertical lines and no interaction between adjacent subsections is considered. Discharge is obtained by summing the contributions of each subsection, obtained by applying the Manning formula:

$$q = \sum_i q_i = \sum_i \frac{R_i^{2/3} A_i}{n_i} \sqrt{S_f} \tag{2},$$

where q is the total discharge, A_i , R_i and n_i are the area, the hydraulic radius and the Manning's roughness coefficient of each sub section i of a compound channel and S_f is the energy slope, assumed constant across the river section. *DCM* is extensively applied in most of the commercial codes, two of them cited in the introduction.

In order to model the interaction between adjacent subsections of a compound section, the Reynolds and the continuity equations can be coupled (Shiono and Knight, 1991), to get:

$$\rho \frac{\partial}{\partial y}\left(H\overline{U}_v \overline{V}_d\right) = \rho g H S_0 + \frac{\partial}{\partial y}\left(H\bar{\tau}_{xy}\right) - \tau_b \left(1+\frac{1}{s^2}\right)^{1/2} \tag{3},$$

where ρ is the water density, g is the gravity acceleration, y is the abscissa according to the lateral direction, U and V are respectively the velocity components along the flow x direction and the lateral y direction, H is the water depth, the sub-index d marks the vertically averaged quantities and the bar the time average along the turbulence period, S_0 is the bed slope, s is the section lateral slope, and τ_β is the bed shear stress. The $\bar{\tau}_{xy}$ turbulent stress is given by the eddy viscosity equation, that is:

$$\bar{\tau}_{xy} = \rho \bar{\varepsilon}_{xy} \frac{\partial U_d}{\partial y} \tag{4a},$$

$$\bar{\varepsilon}_{xy} = \lambda U_* H \tag{4b},$$

where the friction velocity U_* is set equal to:

$$U_* = \left(\frac{f}{8g}\right)^{1/2} U_d \tag{5},$$

206 and f is the friction factor, depending on the bed material. The analytical solution of
207 Eqs. (3)-(5) can be found only if the left hand side of Eq. (3) is zero, which is
208 equivalent to neglecting secondary flows. Other solutions can only be found by
209 assuming a known Γ value for the lateral derivative. Moreover, λ is another
210 experimental factor depending on the section geometry. The result is that solution of
211 Eq. (3) strongly depends on the choice of two coefficients, λ and Γ, which are
212 additional unknowns with respect to the friction factor *f*.
213 In order to reduce to one the number of empirical parameters (in addition to *f*) Huthoff
214 et al. (2008) proposed the so-called Interactive Divided Channel Method (*IDCM*).
215 Integration of Eq. (3) over each i^{th} subsection, neglecting the averaged flow lateral
216 momentum, leads to:

217 $$\rho g A_i S_0 = \rho f_i P_i U_i^2 + \tau_{i+1} H_{i+1} + \tau_i H_i \qquad (6),$$

218 where the left-hand side of Eq.(6) is the gravitational force per unit length,
219 proportional to the density of water ρ, to the gravity acceleration g, to the cross-
220 sectional area A_i, and to the stream wise channel slope S_0. The terms at the right-hand
221 side are the friction forces, proportional to the friction factor f and to the wet solid
222 boundary P_i, as well as the turbulent lateral momentum on the left and right sides,
223 proportional to the turbulent stress τ and to the water depth H.
224 Turbulent stresses are modelled quite simply as:

225 $$\tau_{i+1} = \frac{1}{2}\rho\alpha\left(U_{i+1}^2 - U_i^2\right) \qquad (7),$$

226 where α is a dimensionless interface coefficient, $U^2{}_i$ is the square of the vertically
227 averaged velocity and τ_i is the turbulent stress along the plane between subsection *i-1*
228 and *i*. If subsection *i* is the first (or the last) one, velocity U_{i-1} (or U_{i+1}) is set equal to
229 zero.
230 Following a wall-resistance approach (Chow, 1959), the friction factor f_i is computed
231 as:

232 $$f_i = \frac{g\, n_i^2}{R_i^{1/3}} \qquad (8),$$

233 where n_i is the Manning's roughness coefficient and $R_i(=A_i/P_i)$ is the hydraulic radius
234 of subsection *i*.

Equations (6) forms a system with an order equal to the number m of subsections, which is linear in the U_i^2 unknowns. The results are affected by the choice of the α coefficient, which is recommended by Huthoff et al. (2008), on the basis of lab experiments, equal to 0.02. Computation of the velocities U_i makes it easy to estimate discharge q.

IDCM has the main advantage of using only two parameters, the f and α coefficients. On the other hand, it can be easily shown that α, although it is dimensionless, depends on the way the original section is divided. The reason is that the continuous form of Eq. (6) is given by:

$$\rho g\left(HS_0 - \frac{f\,U^2}{g\,cos\theta} \right) = \frac{\partial}{\partial y}(\tau H) \tag{9},$$

where θ is the bed slope in the lateral direction. Following the same approach as the *IDCM*, if we assume the turbulent stress τ to be proportional to both the velocity gradient in the lateral direction and to the velocity itself, we can write the right-hand side of Eq. (9) in the form:

$$\frac{\partial}{\partial y}(\tau H) = \frac{\partial}{\partial y}\left(\frac{\alpha_H}{2} \rho U \frac{\partial U}{\partial y} H \right) \tag{10},$$

and Eq. (9) becomes:

$$\rho\left(gHS_0 - \frac{f\,U^2}{g\,cos\theta} \right) = \frac{\partial}{\partial y}\left(H \frac{\partial}{\partial y}\left(\alpha_H \rho U^2 \right) \right) \tag{11}.$$

In Eq. (10) α_H is no longer dimensionless, but is a length. To get the same Huthoff formula from numerical discretization of Eq. (10), we should set:

$$\alpha_H = 0.02\,\Delta y \tag{12},$$

where Δy is the subsection width, i.e. the integration step size. This implies that the solution of Eq. (11), according to the Huthoff formula, depends on the way the equation is discretized and the turbulence stress term on the r.h.s. vanishes along with the integration step size.

3 The new methods

3.1 Integrated Channel Method (INCM)

INCM derives from the *IDCM* idea of evaluating the turbulent stresses as proportional to the gradient of the squared averaged velocities, leading to Eqs. (7) and (11). Observe that dimensionless coefficient α, in the stress computation given by Eq. (7), can be written as the ratio between α_H and the distance between verticals *i* and *i+1*. For this reason, coefficient α_H can be thought of as a sort of mixing length, related to the scale of the vortices with horizontal axes. *INCM* assumes the optimal α_H to be proportional to the local water depth, because water depth is at least an upper limit for this scale, and the following relationship is applied:

$$\alpha_H = \xi H \quad (13),$$

where ξ is an empirical coefficient to be further estimated.

3.2 Local hydraulic radius method (LHRM)

LHRM derives from the observation that, in the Manning equation, the average velocity is set equal to:

$$V = \frac{R^{2/3}}{n}\sqrt{S_0} \quad (14),$$

and has a one-to-one relationship with the hydraulic radius. In this context the hydraulic radius has the meaning of a global parameter, measuring the interactions of the particles along all the section as the ratio between an area and a length. The inconvenience is that, according to Eq. (14), the vertically averaged velocities in points very far from each other remain linked anyway, because the infinitesimal area and the infinitesimal length around two verticals are summed to the numerator and to the denominator of the hydraulic radius independently from the distance between the two verticals. To avoid this, *LHRM* computes the discharge as an integral of the vertically averaged velocities, in the following form:

$$q = \int_0^L h(y)U(y)dy \quad (15),$$

where *U* is set equal to:

$$U = \frac{\Re_l^{2/3}}{n}\sqrt{S_0} \tag{16},$$

and $\Re_l$ is defined as local hydraulic radius, computed as:

$$\Re_l(y) = \frac{\int_a^b h(s)\,N(y,s)\,ds}{\int_a^b N(y,s)\sqrt{ds^2+dz^2}} \tag{17a},$$

$$a = \max(0,\ y - \beta h) \tag{17b},$$

$$b = \min(L,\ y + \beta h) \tag{17c},$$

where z is the topographic elevation (function of s), β is an empirical coefficient and L is the section top width. Moreover $N(y, s)$ is a shape function where:

$$N(y,s) = \begin{cases} -\dfrac{\left[y-\beta h(y)\right]-s}{\beta h(y)} & \text{if} \quad a < s < y \\ \dfrac{\left[y-\beta h(y)\right]-s}{\beta h(y)} & \text{if} \quad b > s > y \\ 0 & \text{otherwise} \end{cases} \tag{18}.$$

Equations (18) show how the influence of the section geometry, far from the abscissa y, continuously decreases up to a maximum distance, which is proportional to the water depth according to an empirical positive coefficient β. After numerical discretization, Eqs (15)-(17) can be solved to get the unknown q, as well as the vertically averaged velocities in each subsection. If β is close to zero and the size of each subsection is common for both formulas, LHRM is equivalent to DCM; if β is very large LHRM is equivalent to the traditional Manning formula. In the following, β is calibrated using experimental data available in the literature. A sensitivity analysis is also carried out, to show that the estimated discharge is only weakly dependent on the choice of the β coefficient, far from its possible extreme values.

3.3 Evaluation of the ξ and β parameters by means of lab experimental data

INCM and *LHRM* parameters were calibrated by using data selected from six series of experiments run at the large scale Flood Channel Facility (FCF) of HR Wallingford (UK), (Knight and Sellin, 1987; Shiono and Knight, 1991; Ackers, 1993), as well as

from four series of experiments run in the small-scale experimental apparatus of the Civil Engineering Department at the University of Birmingham (Knight and Demetriou, 1983). The FCF series were named F1, F2, F3, F6, F8 and F10; the Knight and Demetriou series were named K1, K2, K3 and K4. Series F1, F2, and F3 covered different floodplain widths, while series F2, F8, and F10 kept the floodplain widths constant, but covered different main channel side slopes. Series F2 and F6 provided a comparison between the symmetric case of two floodplains and the asymmetric case of a single floodplain. All the experiments of Knight and Demetriou (1983) were run with a vertical main channel wall, but with different B/b ratios. The series K1 has B/b = 1 and its section is simply rectangular. The B/b ratio, for Knight's experimental apparatus, was varied by adding an adjustable side wall to each of the floodplains either in pairs or singly to obtain a symmetrical or asymmetrical cross section. The geometric and hydraulic parameters are shown in Table 1; all notations of the parameters can be found in Fig. 1 and S_0 is the bed slope. The subscripts "mc" and "fp" of the side slope refer to the main channel and floodplain, respectively. Perspex was used for both main flume and floodplains in all tests. The related Manning roughness is 0.01 $m^{-1/3}s$.

The experiments were run with several channel configurations, differing mainly for floodplain geometry (widths and side slopes) and main channel side slopes (see Table 1). The K series were characterized by vertical main channel walls. More information concerning the experimental setup can be found in Table 1 (Knight and Demetriou, 1983; Knight and Sellin, 1987; Shiono and Knight, 1991).

Four series, named F1, F2, F3 and F6, were selected for calibration of the β coefficient, using the Nash Sutcliffe (NS) index of the measured and the computed flow rates as a measure of the model's performance (Nash and Sutcliffe, 1970).

The remaining three series, named F2, F8 and F10, plus four series from Knight and Demetriou, named K1, K2, K3 and K4, were used for validation (no.) 1, as reported in the next section. NS is given by:

$$NS = \left[1 - \frac{\sum_{j=1,2} \sum_{i=1,N_J} \sum_{K=1,M_{NJ}} (q_{i,j,k}^{obs} - q_{i,j,k}^{sim})^2}{\sum_{j=1,2} \sum_{i=1,N_J} \sum_{K=1,M_{NJ}} (q_{i,j,k}^{obs} - \overline{q_{i,j,k}^{obs}})^2} \right] \quad (19),$$

where N_j is the number of series, M_{Nj} is the number of tests for each series, $q^{sim}{}_{i,j,k}$ and $q^{obs}{}_{i,j,k}$ are respectively the computed and the observed discharge (j = 1 for the

339 FCF series and j = 2 for the Knight series; i is the series index and K is the water
340 depth index). $\overline{q_{i,j,k}^{obs}}$ is the average value of the measured discharges.
341 Both ξ and β parameters were calibrated by maximizing the Nash Sutcliffe (NS)
342 index, computed using all the data of the four series used for calibration. See the NS
343 versus ξ and β curves in Figs. 2a and 2b.
344 Calibration provides optimal ξ and β coefficients respectively equal to 0.08 and 9.
345 The authors will show in the next sensitivity analysis that even a one-digit
346 approximation of the ξ and β coefficients provides a stable discharge estimation.

347 *3.4 Sensitivity analysis*

348 We carried out a discharge sensitivity analysis of both new methods using the
349 computed ξ = 0.08 and β=9 optimal values and the data of the F2 and K4 series.
350 Sensitivities were normalized in the following form:

351 $$I_s = \frac{1}{q_{INCM}} \frac{\Delta q}{\Delta \xi} \quad (20),$$

352 $$L_s = \frac{1}{q_{LHRM}} \frac{\Delta q}{\Delta \beta} \quad (21),$$

353

354 where Δq is the difference between the discharges computed using two different β and
355 ξ values. The assumed perturbations"Δβ" and "Δξ" are respectively Δβ = 0.001 β, Δξ
356 = 0.001 ξ.
357 The results of this analysis are shown in Table 2a for the F2 series, where H is the
358 water depth and Q_{meas} the corresponding measured discharge.
359 They show very low sensitivity of both the *INCM* and *LHRM* results, such that a one
360 digit approximation of both model parameters (ξ and β) should guarantee a computed
361 discharge variability of less than 2%.
362 The results of the sensitivity analysis, carried out for series K4 and shown in Table
363 2b, are similar to the previous ones computed for F2 series.

4 Validation criterion

4.1 Validation n.1 - Comparison with laboratory experimental data

A first validation of the two methods was carried out by using the calibrated parameter values, the same Nash-Sutcliffe performance measure and all the available experimental series. The results were also compared with results of *DCM* and *IDCM* methods, the latter applied using the suggested $\alpha = 0.02$ value and five subsections, each one corresponding to a different bottom slope in the lateral y direction. The NS index for all data series is shown in Table 3.

The *DCM* results are always worse and are particularly bad for all the K series. The results of both the *IDCM* and *INCM* methods are very good for the two F series not used for calibration, but are both poor for the K series. The *LHRM* method is always the best and also performs very well in the K series. The reason is probably that the K series tests have very low discharges, and the constant $\alpha = 0.02$, the coefficient adopted in the *IDCM* method, does not fit the size of the subsections and Eq. (13) is not a good approximation of the mixing length α_H in Eq. (12) for low values of the water depth. In Figs. 3a and 3b the NS curves obtained by using *DCM*, *IDCM*, *INCM* and *LHRM*, for series F2 and K4, are shown.

4.2 Validation n.2 - Comparison with field data

Although rating curves are available in different river sites around the world, field validation of the uniform flow formulas is not easy, for at least two reasons:

1) The average friction factor f and the related Manning's coefficient are not known as in the lab case and the results of all the formulas need to be scaled according to the Manning's coefficient to be compared with the actually measured discharges;

2) River bed roughness does change, along with the Manning's coefficient, from one water stage to another (it usually increases along with the water level).

A possible way to circumvent the problem is to apply the compared methods in the context of a calibration problem, where both the average Manning's coefficient and the discharge hydrograph are computed from the known level hydrographs measured in two different river cross sections (Perumal et al., 2007; Aricò et al., 2009). The authors solved the diffusive wave simulation problem using one known level

394 hydrograph as the upstream boundary condition and the second one as the benchmark
395 downstream hydrograph for the Manning's coefficient calibration.
396 It is well-known in the parameter estimation theory (Aster et al., 2012) that the
397 uncertainty of the estimated parameters (in our case the roughness coefficient) grows
398 quickly with the number of parameters, even if the matching between the measured
399 and the estimated model variables (in our case the water stages in the downstream
400 section) improves. The use of only one single parameter over all the computational
401 domain is motivated by the need of getting a robust estimation of the Manning's
402 coefficient and of the corresponding discharge hydrograph.
403 Although the accuracy of the results is restricted by several modeling assumptions, a
404 positive indication about the robustness of the simulation model (and the embedded
405 relationship between the water depth and the uniform flow discharge) is given by: 1)
406 the match between the computed and the measured discharges in the upstream
407 section, 2) the compatibility of the estimated average Manning's coefficient with the
408 site environment.
409 The area of interest is located in the Alzette River basin (Gran-Duchy of
410 Luxembourg) between the gauged sections of Pfaffenthal and Lintgen (Fig. 4). The
411 river reach length is about 19 km, with a mean channel width of ~30 m and an
412 average depth of ~4 m. The river meanders in a relatively large and flat plain about
413 300 m, with a mean slope of ~0.08%.

414 The methodology was applied to a river reach 13 Km long, between two instrumented
415 sections, Pfaffenthal (upstream section) and Hunsdorf (downstream section), in order
416 to have no significant lateral inflow between the two sections.
417 Events of January 2003, January 2007 and January 2011 were analysed. For these
418 events, stage records and reliable rating curves are available at the two gauging
419 stations of Pfaffenthal and Hunsdorf. The main hydraulic characteristics of these
420 events, that is duration (Δt), peak water depth (H_{peak}) and peak discharge (q_{peak}), are
421 shown in Table 4.
422 In this area a topographical survey of 125 river cross sections was available. The
423 hydrometric data were recorded every 15 min. The performances of the discharge
424 estimation procedures were compared by means of the Nash Suctliffe criterion.
425 The results of the *INCM* and *LHRM* methods were also compared with those of the
426 *DCM* and *IDCM* methods, the latter applied by using α = 0.02 and an average

427 subsection width equal to 7 m. The computed average Manning's coefficients n_{opt},
428 reported in Table 5, are all consistent with the site environment, although they attain
429 very large values, according to *DCM* an *IDCM*, in the 2011 event.
430 The estimated and observed dimensionless water stages in the Hunsdorf gauged site,
431 for 2003, 2007 and 2011 events are shown in Figs. 5-7.
432 Only the steepest part of the rising limb, located inside the colored window of each
433 Figure, was used for calibration. The falling limb is not included, since it has a lower
434 slope and is less sensitive to the Manning's coefficient value.
435 A good match between recorded and simulated discharge hydrographs can be
436 observed (Figs. 8-10) in the upstream gauged site for each event.
437 For all investigated events the Nash Sutcliffe efficiency NS_q is greater than 0.90, as
438 shown in Table 6.
439 The error obtained between measured and computed discharges, with all methods, is
440 of the same order of the discharge measurement error. Moreover, this measurement
441 error is well known to be much larger around the peak flow, where the estimation
442 error has a larger impact on the NS coefficient. The NS coefficients computed with
443 the *LHRM* and *INCM* methods are anyway a little better than the other two.

444 *4.3 Validation n.3 - Comparison with results of 3D ANSYS CFX solver*

445 The vertically averaged velocities computed using *DCM*, *IDCM*, *INCM* and *LHRM*
446 were compared with the results of the well known ANSYS 3D code, named CFX,
447 applied to a prismatic reach with the irregular cross-section measured at the Hunsdorf
448 gauged section of the Alzette river. The length of the reach is about four times the top
449 width of the section.
450 In the homogeneous multiphase model adopted by CFX, water and air are assumed to
451 share the same dynamic fields of pressure, velocity and turbulence and water is
452 assumed to be incompressible. CFX solves the conservation of mass and momentum
453 equations, coupled with the air pressure-density relationship and the global continuity
454 equation in each node. Call α_l, ρ_l, μ_l and $\mathbf{U}_l$ respectively the volume fraction, the
455 density, the viscosity and the time averaged value of the velocity vector for phase l (l
456 = w (water), a (air)), that is:

457 $$\rho = \sum_{l=w,a} \alpha_l \rho_l \qquad (22a),$$

458 $$\mu = \sum_{l=w,a} \alpha_l \mu_l \quad (22b),$$

459 where ρ and μ are the density and the viscosity of the "averaged" phase. The air
460 density is assumed to be a function of the pressure *p*, according to the state equation:

461 $$\rho_a = \rho_{a,0} e^{\gamma(p-p_o)} \quad (22c),$$

462 where the sub-index 0 marks the reference state values and γ is the air compressibility
463 coefficient.
464 The governing equations are the following: 1) the mass conservation equation, 2) the
465 Reynolds averaged continuity equation of each phase and 3) the Reynolds averaged
466 momentum equations. Mass conservation implies:

467 $$\sum_{l=w,a} \alpha_l = 1 \quad (23).$$

468 The Reynolds averaged continuity equation of each phase *l* can be written as:

469 $$\frac{\partial \rho_l}{\partial t} + \nabla \cdot (\rho_l \, \mathbf{U}) = S_l \quad (24),$$

470 where S_l is an external source term. The momentum equation instead refers to the
471 "averaged" phase and is written as:

472 $$\frac{\partial (\rho \mathbf{U})}{\partial t} + \nabla \cdot (\rho \mathbf{U} \otimes \mathbf{U}) - \nabla \cdot \left(\mu_{eff} \left(\nabla \mathbf{U} + (\nabla \mathbf{U})^T \right) \right) + \nabla p' = S_M \quad (25),$$

473 where $\otimes$ is the dyadic symbol, S_M is the momentum of the external source term *S*, and
474 μ_{eff} is the effective viscosity accounting for turbulence and defined as:

475 $$\mu_{eff} = \mu + \mu_t \quad (26),$$

476 where μ_t is the turbulence viscosity and p' is the modified pressure, equal to:

477 $$p' = p + \frac{2}{3} \rho k + \frac{2}{3} \mu_{eff} \nabla \cdot \mathbf{U} \quad (27),$$

478 where *k* is the turbulence kinetic energy, defined as the variance of the velocity
479 fluctuations and *p* is the pressure. Both phases share the same pressure *p* and the same
480 velocity $\mathbf{U}$.
481 To close the set of six scalar equations (Eq.23, Eq.24 (two) and Eq.25 (three)), we
482 finally apply the *k*-ε turbulence model implemented in the CFX solver. The

483 implemented turbulence model is a two equation model, including two extra transport
484 equations to represent the turbulent properties of the flow.
485 Two-equation models account for history effects like convection and diffusion of
486 turbulent energy. The first transported variable is turbulent kinetic energy, k; the
487 second transported variable is the turbulent dissipation, ε. The K-epsilon model has
488 been shown (Jones, 1972; Launder, 1974) to be useful for free-shear layer flows with
489 relatively small pressure gradients. Similarly, for wall-bounded and internal flows, the
490 model gives good results, but only in cases where the mean pressure gradients are
491 small.
492 The computational domain was divided using both tetrahedral and prismatic elements
493 (Fig. 11). The prismatic elements were used to discretize the computational domain in
494 the near-wall region over the river bottom and the boundary surfaces, where a
495 boundary layer is present, while the tetrahedral elements were used to discretize the
496 remaining domain. The number of elements and nodes, in the mesh used for the
497 specific case are of the order respectively $4*10^6$ and $20*10^6$.
498 A section of the mesh is shown in Fig.12. The quality of the mesh was verified by
499 using a pre-processing procedure by ANSYS® ICEM CFD™ (Ansys inc., 2006).
500 The six unknowns in each node are the pressure, the velocity components, and the
501 volume fractions of the two phases. At each boundary node three of the first four
502 unknowns have to be specified. In the inlet section a constant velocity, normal to the
503 section, is applied, and the pressure is left unknown. In the outlet section the
504 hydrostatic distribution is given, the velocity is assumed to be still normal to the
505 section and its norm is left unknown. All boundary conditions are reported in Table 7.
506 The opening condition means that that velocity direction is set normal to the surface,
507 but its norm is left unknown and a negative (entering) flux of both air and water is
508 allowed. Along open boundaries the water volume fraction is set equal to zero. The
509 solution of the problem converges towards two extremes: nodes with zero water
510 fraction, above the water level, and nodes with zero air fraction below the water level.
511 On the bottom boundary, between the nodes with zero velocity and the turbulent flow
512 a boundary layer exists that would require the modelling of micro scale irregularities.
513 CFX allows the use, inside the boundary layer, of a velocity logarithmic law,
514 according to an equivalent granular size. The relationship between the granular size
515 and the Manning's coefficient, according to Yen (1994), is given by:

516 $$d_{50} = \left(\frac{n}{0.0474}\right)^6 \quad (28),$$

517 where d_{50} is the average granular size to be given as the input in the CFX code.
518 Observe that the assumption of known and constant velocity directions in the inlet and
519 outlet section is a simplification of reality. A more appropriate boundary condition at
520 the outlet section, not available in the CFX code, would have been given by zero
521 velocity and turbulence gradients (Rameshwaran et al. 2013). For this reason, a better
522 reconstruction of the velocity field can be found in an intermediate section, where
523 secondary currents with velocity components normal to the mean flow direction can
524 be easily detected (Peters and Goldberg, 1989; Richardson and Colin, 1996). See in
525 Fig. 13 how the intermediate section was divided to compute the vertically averaged
526 velocities in each segment section and, in Fig.14, the velocity components tangent to
527 the cross section plane.
528 These 3D numerical simulations confirm that the momentum Γ, proportional to the
529 derivative of the average tangent velocities and equivalent to the left hand side of Eq.
530 2, cannot be set equal to zero, if a rigorous reconstruction of the velocity field is
531 sought after.
532 To compute the uniform flow discharge, for a given outlet section, CFX code is run
533 iteratively, each time with a different average longitudinal velocity in the inlet section,
534 until the same water depth as in the outlet section is attained in the inlet section for
535 steady state conditions.Using the velocity distribution computed in the middle section
536 along the steady state computation as upstream boundary condition, transient analysis
537 is carried on until pressure and velocity oscillations become periodic.
538 In order to test the achievement of the fully developed state within the first half of the
539 modeled length the authors plotted the vertical profiles of the streamwise velocity
540 components for ten verticals, equally spaced along the longitudinal axis of the main
541 channel. See in Fig.15 the plot of four of them and their location. The streamwise
542 velocity evolves longitudinally and becomes almost completely self similar starting
543 from the vertical line in the middle section.
544 Stability of the results has been finally checked against the variation of the length of
545 the simulated channel. The dimensionless sensitivity of the discharge with respect to
546 the channel length is equal to 0.2%.

547 See in Table 8 the comparison between the vertically averaged state velocities,
548 computed through the *DCM*, *IDCM*, *INCM*, *LHRM* formulas (u_{DCM}, u_{IDCM}, u_{INCM},
549 u_{LHRM}) and through the CFX code (u_{CFX}). Table 9 also shows the relative difference,
550 Δu, evaluated as:

551 $$\Delta u = \frac{u - u_{CFX}}{u_{CFX}} \times 100 \quad (29),$$

552 As shown in Table 8, both *INCM* and *LHRM* perform very well in this validation test
553 instead of *DCM*, which clearly overestimates averaged velocities. In the central area
554 of the section the averaged velocities calculated by the *INCM*, *LHRM* and CFX code
555 are quite close with a maximum difference ~7%. By contrast, larger differences are
556 evident close to the river bank, in segments 1 and 9, where *INCM* and *LHRM*
557 underestimate the CFX values. These larger differences show the limit of using a 1D
558 code. Close to the bank the wall resistance is stronger and the velocity field is more
559 sensitive to the turbulent exchange of energy with the central area of the section,
560 where higher kinetic energy occurs. Thanks to the simulation of secondary flows (see
561 Fig. 14) CFX allows this exchange and the related mixing. However, because the
562 near-bank subsections are characterised by small velocities, their contribution to the
563 global discharge and bed load is relatively small.

564 **5 Conclusions**

565 Two new methods computing the vertically averaged velocities along irregular
566 sections have been presented. The first method, named *INCM*, develops from the
567 original *IDCM* method and it is shown to perform better than the previous one, with
568 the exception of lab tests with very small discharge values. The second one, named
569 *LHRM*, has empirical bases, and gives up the ambition of estimating turbulent
570 stresses, but has the following important advantages:

571 1. It relies on the use of only two parameters: the friction factor f (or the
572 corresponding Manning's coefficient n) and a second parameter βwhich on the basis
573 of the available laboratory data was estimated to be equal to 9.

574 2. The β coefficient has a simple and clear physical meaning: the correlation distance,
575 measured in water depth units, of the vertically averaged velocities between two
576 different verticals of the river cross-section.

3. The sensitivity of the results with respect to the model β parameter was shown to be very low, and a one digit approximation is sufficient to get a discharge variability less than 2%. A fully positive validation of the method was carried out using lab experimental data, as well as field discharge and roughness data obtained by using the unsteady-state level analysis proposed by Aricò et al. (Aricò et al., 2009) and applied to the Alzette river, in the grand Duchy of Luxembourg.

4. Comparison between the results of the CFX 3D turbulence model and the *LHRM* model shows a very good match between the two computed total discharges, although the vertically averaged velocities computed by the two models are quite different near to the banks of the river.

Moreover, the estimation of the velocity profiles in each of the considered sub-sections could be used in order to evaluate the vertical average velocity and so the shear stresses at the boundary of the whole cross section. In fact, it is well-known that bed load transport is directly related to the bed shear stress and that this is proportional in each point of the section to the second power of the vertically averaged velocity, according to Darcy Weisbach (Ferguson, 2007):

$$\tau_0 = \rho U^2 \frac{f}{8} \qquad (30),$$

Moreover, it is well-known that bed load transport is directly related to the bed shear stress and that this is proportional in each point of the section to the second power of the vertically averaged velocity, according to Darcy Weisbach formula (Ferguson, 2007):

$$\tau_0 = \rho U^2 \frac{f}{8} \qquad (30),$$

All the bed load formulas available in literature compute the solid flux per unit width. For example, the popular Schoklisch formula (Gyr et al., 2006) is:

$$q_s = \frac{2.5}{\rho_s / \rho} S^{\frac{3}{2}} (q - q_c) \qquad (31),$$

where q and q_s are respectively the liquid and the solid discharge per unit width. This implies that the information given by the mean velocity and by the cross section geometry is not sufficient for a good estimation of the bed load in irregular sections. If Eq.(31) holds, the error in the bed load estimation is proportional to the error in the volumetric discharge, discussed in the previous sections.

Acknowledgements

The authors wish to express their gratitude to the Administration de la gestionde l'eau of Grand-Duché de Luxembourg and the Centre de Recherche Public "Gabriel Lippmann" for providing hydrometric and topographical data on Alzette River.

Notation

A_i = area of each subsection “i” of a compound channel

B = top width of compound channel

b = main channel width at bottom

f = friction factor

g = gravity acceleration

H = total depth of a compound channel

n_{mc} and n_{fp}= Manning’s roughness coefficient for the main channel and floodplain, respectively

P_i = wetted perimeter of each subsection “i” of a compound channel

Q_{meas}= measured discharge

R_i = hydraulic radius of each subsection “i” of a compound channel

S_0 = longitudinal channel bed slope

S_f = energy slope

τ = turbulent stress

ε = turbulent dissipation

ρ = fluid density

μ = fluid viscosity

α = *IDCM* interface coefficient

β = *LHRM* coefficient

ξ = *INCM* coefficient

635

636 **References**

637

638 Abril, J. B., and Knight, D. W. (2004). Stage-discharge prediction for rivers in flood
639 applying a depth-averaged model. *J. Hydraul. Res*., 42(6), 616–629.
640
641 Ansys Inc., Canonsburg. (2006). ANSYS CFX Reference guide.
642
643 Ackers, P. (1993). Flow formulae for straight two-stage channels. *J. Hydraul. Res.*,
644 31(4), 509–531.
645
646 Aricò, C. and Tucciarelli, T. (2007). A Marching in Space and Time (MAST) solver
647 of the shallow water equations. Part I: the 1D model. Advances in Water Resources,
648 30(5), 1236-1252.
649
650 Aricò, C., Nasello, C. and Tucciarelli, T. (2009). Using unsteady water level data to
651 estimate channel roughness and discharge hydrograph, *Advances in Water Resources*;
652 32(8), 1223-1240.
653
654 Aster, C., Borchers, B., Clifford, H. (2012). Parameter Estimation and Inverse
655 Problems. Elsevier, ISBN: 978-0-12-385048-5.
656
657 Bousmar, D., and Zech, Y. (1999). Momentum transfer for practical flow computation
658 in compound channels. *J. Hydraul. Eng.*; 696–706.
659
660 Cao, Z., Meng, J., Pender, G., & Wallis, S. (2006). Flow resistance and momentum
661 flux in compound open channels. *J. Hydraul. Eng.*; 1272–1282.
662
663 Chow, V. T. (1959). Open channel hydraulics. New York: McGraw-Hill.
664

665 Corato, G., Moramarco, T., and Tucciarelli, T. (2011). Discharge estimation
666 combining flow routing and occasional measurements of velocity, *Hydrol. Earth Syst.*
667 *Sci.*,15, pp. 2979-2994.
668
669 Dey, M., and Lambert, M. F. (2006). Discharge prediction in compound channels by
670 end depth method. *J. Hydraul. Res.,*44(6), 767–776.
671
672 Ferguson, R. (2007) Flow resistance equations for gravel and boulder-bed streams.
673 *Water resources research*, 43, W05427.
674
675 Gyr, A, and Hoyer k. (2006), Sediment Transport A geophysical Phenomenon,
676 Springer, 30-31.
677
678 Herschel, C. (1897). On the origin of the Chezy formula, *J. Assoc. of Engineering*
679 *Soc.* 18, 363-368.
680
681 Hu, C., Ji, Z., and Guo, Q. (2010). Flow movement and sediment transport in
682 compound channels. *J. Hydraul. Res*., 48(1), 23–32.
683
684 Huthoff, F., Roos, P. C., Augustijn, D. C. M., and Hulscher, S. J. M. H. (2008).
685 Interacting divided channel method for compound channel flow. *J. Hydraul. Eng*.,
686 1158–1165.
687
688 Jones, W. P., and Launder, B. E. (1972). The Prediction of Laminarization with a
689 Two-Equation Model of Turbulence*, International Journal of Heat and Mass*
690 *Transfer*; vol. 15, pp. 301-314.
691
692 Kejun Yang, Xingnian Liu; ShuyouCao and Er Huang. (2013). Stage-Discharge
693 Prediction in Compound Channels, *J. Hydraul. Eng.*
694
695 Knight, D. W., and Abril, B. (1996).Refined calibration of a depth averaged model for
696 turbulent flow in a compound channel. *Proc. ICE Water Maritime Energy*; 118(3),
697 151–159.
698

699 Knight, D.W., and Demetriou, J. D. (1983). Flood plain and main channel flow
700 interaction, *J. Hydraul. Eng.*, 1073–1092.
701
702 Knight, D. W., and Hamed, M. E. (1984).Boundary shear in symmetrical compound
703 channels, *J. Hydraul. Eng.*, 1412–1430.
704
705 Knight, D. W., McGahey, C., Lamb, R., and Samuels, P. G. (2010).Practical channel
706 hydraulics: Roughness, conveyance and afflux. CRC Press/Taylor and Francis,
707 Leiden, The Netherlands, 1–354.
708
709 Knight, D. W., and Sellin, R. H. J. (1987). The SERC flood channel facility. *J. Inst.*
710 *Water Environ.* Manage, 1(2), 198–204.
711
712 Knight, D. W., and Shiono, K. (1996). River channel and floodplain hydraulics.
713 Chapter 5, Floodplain processes, M. G. Anderson,D. E. Walling, and P. D. Bates,
714 eds., Wiley, New York, 139–181.
715
716 Knight, D. W., Shiono, K., and Pirt, J. (1989).Prediction of depth mean velocity and
717 discharge in natural rivers with overbank flow. Proc., Int. Conf. on Hydraulic and
718 Environmental Modelling of Coastal, Estuarine and River Waters, R. A. Falconer, P.
719 Goodwin and R. G. S. Matthew, eds., Gower Technical, Univ. of Bradford, U.K.,
720 419–428.
721
722 Lambert, M. F., and Sellin, R. H. J. (1996). Discharge prediction in straight
723 compound channels using the mixing length concept. *J.Hydraul. Res.*,34(3), 381–394.
724
725 Launder, B. E., and Sharma, B. I. (1974). Application of the Energy Dissipation
726 Model of Turbulence to the Calculation of Flow Near a Spinning Disc. Letters in Heat
727 and Mass Transfer; vol. 1, no. 2, pp. 131-138.
728
729 Liao, H., and Knight, D. W. (2007). Analytic stage-discharge formulas for flow in
730 straight prismatic channels. *J. Hydraul. Eng.*, 1111–1122.
731

732 Lyness, J. F., Myers, W. R. C., Cassells, J. B. C., and O'Sullivan, J. J. (2001). The
733 influence of planform on flow resistance in mobile bed compound channels *Proc.,*
734 *ICE Water Maritime Eng.*; 148(1), 5–14.
735
736 McGahey, C. (2006). A practical approach to estimating the flow capacity of rivers.
737 Ph.D. thesis, The Open Univ., Milton Keynes, U.K,. (British Library).
738
739 McGahey, C., Knight, D. W., and Samuels, P. G. (2009). Advice, methods and tools
740 for estimating channel roughness. *Proc. ICE Water Manage,* 162(6), 353–362.
741
742 Moreta, P. J. M., and Martin-Vide, J. P. (2010). Apparent friction coefficient in
743 straight compound channels. *J. Hydraul. Res.*, 48(2), 169–177.
744
745 Myers,W. R. C., & Brennan, E. K. (1990). Flow resistance in compound channels. *J.*
746 *Hydraul. Res.*, 28(2), 141–155.
747
748 Omran, M., and Knight, D. W. (2010). Modelling secondary cells and sediment
749 transport in rectangular channels. *J. Hydraul. Res.*, 48(2), 205–212.
750
751 Peters J.J. and Goldberg A. (1989). Flow data in large alluvial channels in
752 Maksimovic, C. &Radojkovic, M. (eds) Computational Modeling and Experimental
753 methods in Hydraulics; Elsevier, London, 77-86.
754

755 Perumal M, Moramarco T, Sahoo B, Barbetta S. (2007). A methodology for discharge
756 estimation and rating curve development at ungauged river sites. *Water Resources*
757 *Res.*
758
759 Rameshwaran, P. and Shiono, K. (2007). Quasi two-dimensional model for straight
760 overbank flows through emergent vegetation on floodplains. . *J. Hydraul. Res. 45(3),*
761 *302-315.*
762
763 Rameshwaran, Ponnambalam; Naden, Pamela; Wilson, Catherine A.M.E.; Malki,
764 Rami; Shukla, Deepak R.; Shiono, Koji. (2013). Inter-comparison and validation of

765 computational fluid dynamics codes in two-stage meandering channel flows. *Applied*
766 *Mathematical Modelling*, 37 (20-21). 8652-8672.
767
768 Rhodes, D. G., and Knight, D. W. (1994). Velocity and boundary shear in a wide
769 compound duct. *J. Hydraul. Res.,*32(5), 743–764.
770
771 Richardson R. W. and Colin R. Thorne. (1998). Secondary Currents around Braid Bar
772 inBrahmaputra River, Bangladesh. *J. Hydraul. Eng.*, 124(3), 325–328.
773
774 Schlichting, H. (1960). Boundary layer theory, 4th Ed., McGraw-Hill,NewYork.
775
776 Sellin, R. H. J. (1964). A laboratory investigation into the interaction between the
777 flow in the channel of a river and that over its flood plain. La Houille Blanche, 7,
778 793–801.
779
780 Shiono, K., Al-Romaih, J. S., and Knight, D. W. (1999). Stage-discharge assessment
781 in compound meandering channels. *J. Hydraul. Eng.*, 66–77.
782
783 Shiono, K., and Knight, D. W. (1991). Turbulent open-channel flows with variable
784 depth across the channel. *J. Fluid Mech.*,222, 617–646.
785
786 Stephenson, D., andKolovopoulos, P. (1990). Effects of momentum transfer in
787 compound channels. *J. Hydraul. Eng.*, 1512–1522.
788
789 Tang, X., and Knight, D. W. (2008). Lateral depth-averaged velocity distributions
790 and bed shear in rectangular compound channels. *J. Hydraul. Eng.*, 1337–1342.
791
792 Van Prooijen, B. C., Battjes, J. A., andUijttewaal, W. S. J. (2005). Momentum
793 exchange in straight uniform compound channel flow. *J. Hydraul. Eng.*, 175–183.
794
795 Wormleaton, P. R., Allen, J., andHadjipanos, P. (1982). Discharge assessment in
796 compound channel flow. *J. Hydraul. Div.*, 108(9), 975–994.
797

798 Wormleaton, P. R., &Hadjipanos, P. (1985). Flow distribution in compound channels.
799 *J. Hydraul. Eng.*, 357–361.
800
801 Yen, B.C. (1992).The Manning formula in context. Channel Flow Resistance:
802 Centennial of Manning's Formula,. Editor Water Resources Publications, Littleton,
803 Colorado, USA, p. 41.
804
805 MIKE11, A Modelling System for Rivers and Channels, Reference Manual, DHI
806 2009
807 HEC-RAS, River Analysis System, Hydraulic Reference Manual, US Army Corps of
808 Engineers 2010.
809

Table 1 Geometric and Hydraulic Laboratory Parameters of the experiment series.

Series	S_0 [‰]	h [m]	B [m]	b_4 [m]	b_1 [m]	b_3 [m]	s_{fp} [-]	s_{mc} [-]
F1	1.027	0.15	1.8	1.5	4.1	4.100	0	1
F2					2.25	2.250	1	1
F3					0.75	0.750	1	1
F6					2.25	0	1	1
F8					2.25	2.250	1	0
F10					2.25	2.250	1	2
K1	0.966	0.08	0.15	0.152	0.229	0.229	0	0
K2					0.152	0.152		
K3					0.076	0.076		
K4					-	-		

Table 2a Sensitivities I_s and L_s computed in the F2 series for the optimal parameter values.

H [m]	Q_{meas}[m^3s^{-1}]	I_s	L_s
0.156	0.212	0.2209	0.2402
0.169	0.248	0.1817	0.2194
0.178	0.282	0.1651	0.2044
0.187	0.324	0.1506	0.1777
0.198	0.383	0.1441	0.1584
0.214	0.480	0.1305	0.1336
0.249	0.763	0.1267	0.1320

823 Table 2b Sensitivities I_s and L_s computed in the K4 series for the optimal parameter
824 values.

H [m]	Q_{meas} [m^3s^{-1}]	I_s	L_s
0.085	0.005	0.3248	0.3282
0.096	0.008	0.2052	0.2250
0.102	0.009	0.1600	0.1709
0.114	0.014	0.1354	0.1372
0.127	0.018	0.1174	0.1208
0.154	0.029	0.0851	0.0866

825

826 Table 3 Nash-Sutcliffe Efficiency for all (calibration and validation) experimental
827 series.

	Series	*DCM*	*IDCM*	*INCM*	*LHRM*
Calibration Set	*F1*	0.7428	0.9807	0.9847	0.9999
	F2	0.6182	0.9923	0.9955	0.9965
	F3	0.7219	0.9744	0.9261	0.9915
	F6	0.7366	0.9733	0.9888	0.9955
Validation Set	*F8*	-0.0786	0.9881	0.9885	0.9964
	F10	-0.0885	0.9965	0.9975	0.9978
	K1	-14.490	-0.7007	-8.2942	0.9968
	K2	-0.9801	0.3452	-1.8348	0.9619
	K3	0.1762	0.6479	-0.3944	0.9790
	K4	0.2878	0.888	0.3548	0.9958

828
829
830
831
832
833
834
835

836 Table 4 Main characteristics of the flood events at the Pfaffenthal and Hunsdorf
837 gauged sites.

Event	Δt [h]	Pfaffenthal		Hunsdorf	
		H_{peak} [m]	q_{peak} [m^3s^{-1}]	H_{peak} [m]	Q_{peak} [m^3s^{-1}]
January 2003	380	3.42	70.98	4.52	67.80
January 2007	140	2.90	53.68	4.06	57.17
January 2011	336	3.81	84.85	4.84	75.10

838

839 Table 5 Optimum roughness coefficient, n_{opt}, for the three flood events.

Event	*DCM* n_{opt} [$sm^{-1/3}$]	*IDCM* n_{opt} [$sm^{-1/3}$]	*INCM* n_{opt} [$sm^{-1/3}$]	*LHRM* n_{opt} [$sm^{-1/3}$]
January 2003	0.054	0.047	0.045	0.045
January 2007	0.051	0.047	0.046	0.045
January 2011	0.070	0.070	0.057	0.055

840

841 Table 6 Nash-Sutcliffe efficiency of estimated discharge hydrographs for the analysed
842 flood events.

Event	*DCM* NS_q [-]	*IDCM* NS_q [-]	*INCM* NS_q [-]	*LHRM* NS_q [-]
January 2003	0.977	0.987	0.991	0.989
January 2007	0.983	0.988	0.989	0.992
January 2011	0.898	0.899	0.927	0.930

843
844
845
846
847
848
849

850 Table 7 Boundary conditions assigned in the CFX simulation.

851

Geometry Face	Boundary Condition
Inlet	All velocity components
Outlet	Velocity direction and hydrostatic pressure distribution
Side-Walls	Opening
Top	Opening
Bottom	No-slip wall condition, with roughness given by equivalent granular size d_{50}.

852

853

854 Table 8 Simulated mean velocities in each segment section using 1D hydraulic
855 models with *DCM*, *IDCM*, *INCM*, *LHRM* and *CFX*, and corresponding differences.

Subsection	u_{CFX} [ms^{-1}]	u_{DCM} [ms^{-1}]	u_{IDCM} [ms^{-1}]	u_{INCM} [ms^{-1}]	u_{LHRM} [ms^{-1}]	Δu_{DCM} [%]	Δu_{IDCM} [%]	Δu_{INCM} [%]	Δu_{LHRM} [%]
1	1.33	1.58	1.47	1.23	1.12	18.79	10.52	-7.52	-15.78
2	1.37	1.42	1.4	1.36	1.38	3.65	2.19	-0.73	0.73
3	1.38	1.53	1.48	1.38	1.4	10.87	7.25	0	1.45
4	1.47	1.64	1.6	1.56	1.57	11.56	8.84	6.13	6.80
5	1.53	1.94	1.8	1.59	1.61	26.79	17.65	3.92	5.23
6	1.57	2.01	1.81	1.6	1.68	28.02	15.29	1.91	7.00
7	1.46	1.66	1.65	1.49	1.5	13.69	13.01	2.05	2.74
8	1.42	1.48	1.46	1.44	1.43	4.22	2.82	1.40	0.70
9	0.88	0.91	0.90	0.70	0.69	3.40	2.27	-20.45	-21.59

856

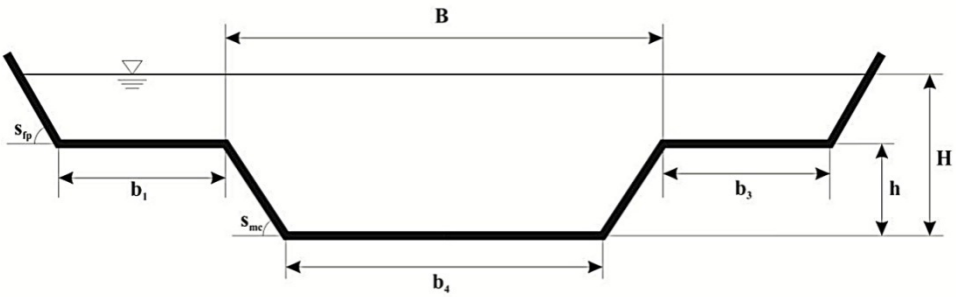

857

858 Figure 1 Compound channel geometric parameters.

859

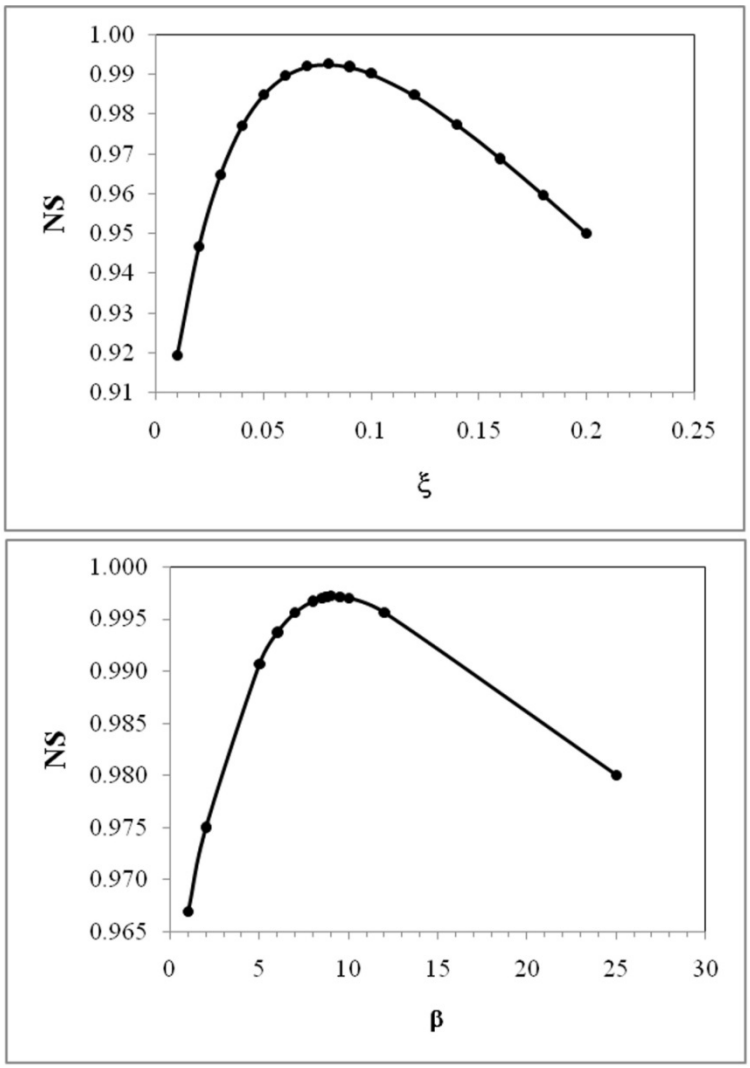

860

861 Figure 2 NS versus ξ and β curves respectively for *INCM* (a) and *LHRM* (b) methods.

862

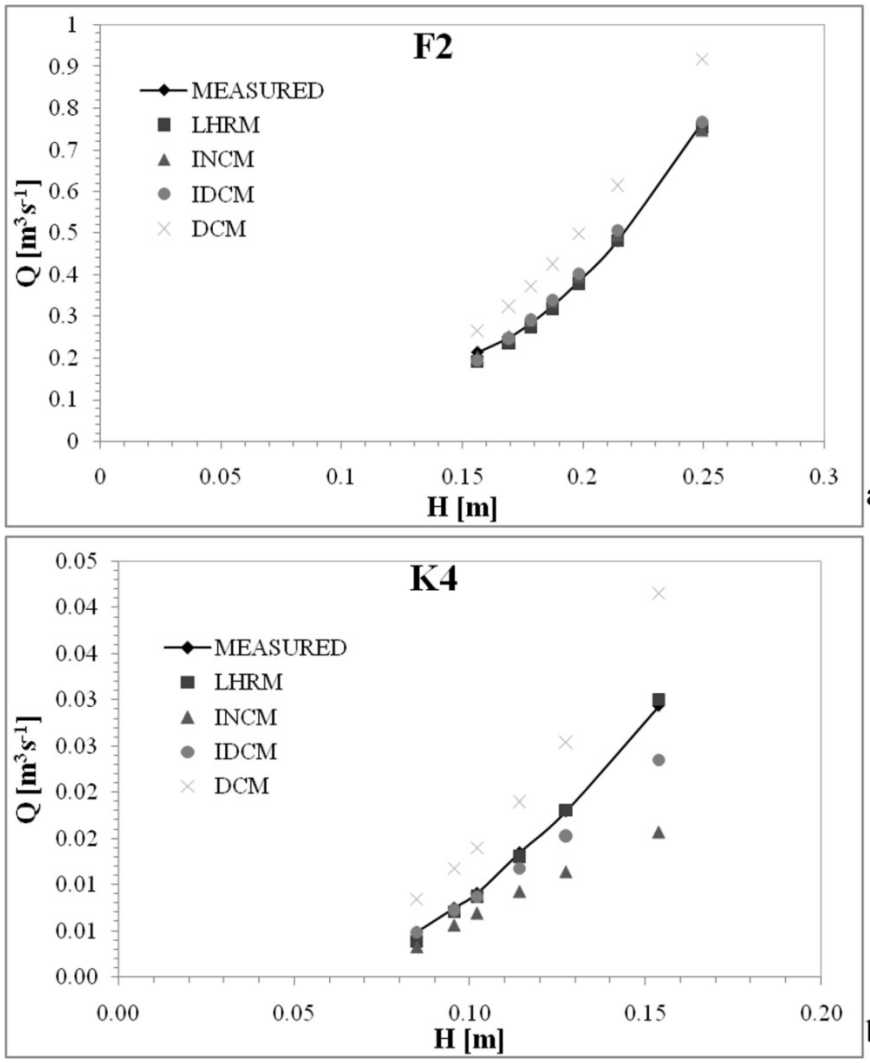

863

864 Figure 3 Estimated discharge values against HR Wallingford FCF measures for F2 (a)
865 and K4 (b) series.

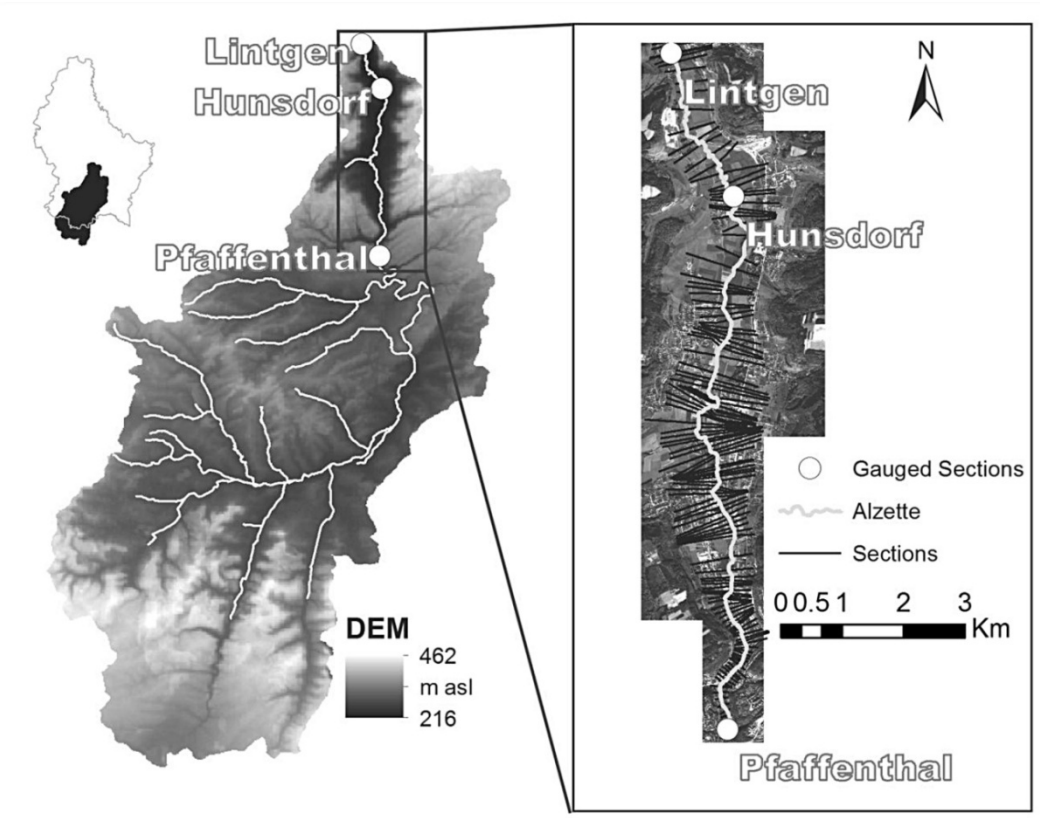

866

867 Figure 4 The Alzette Study Area.

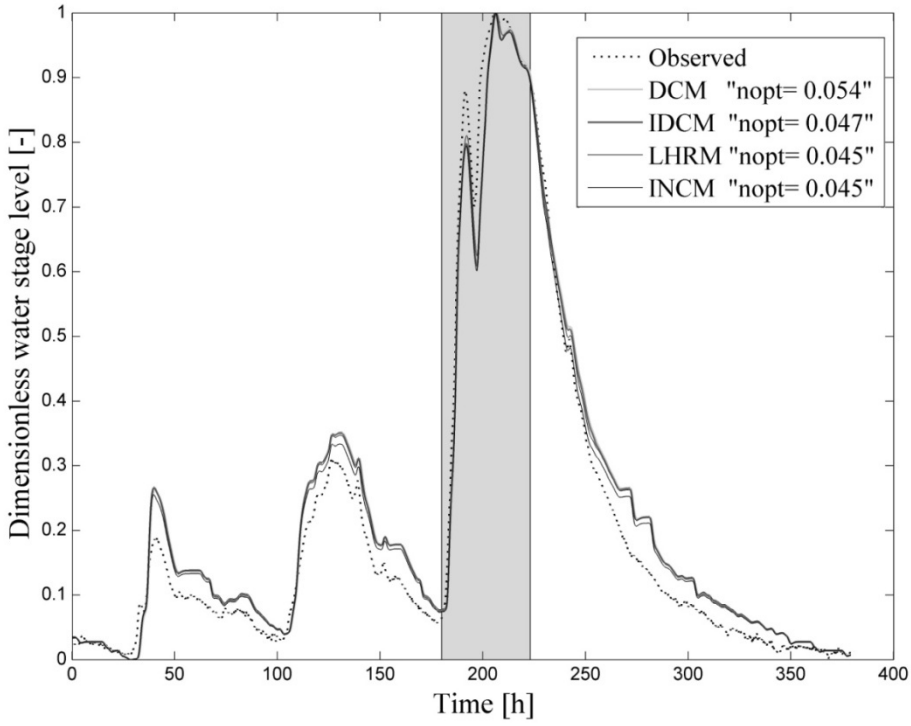

868

869 Figure 5 Observed and simulated stage hydrographs at Hunsdorf gauged site in the
870 event of January 2003.

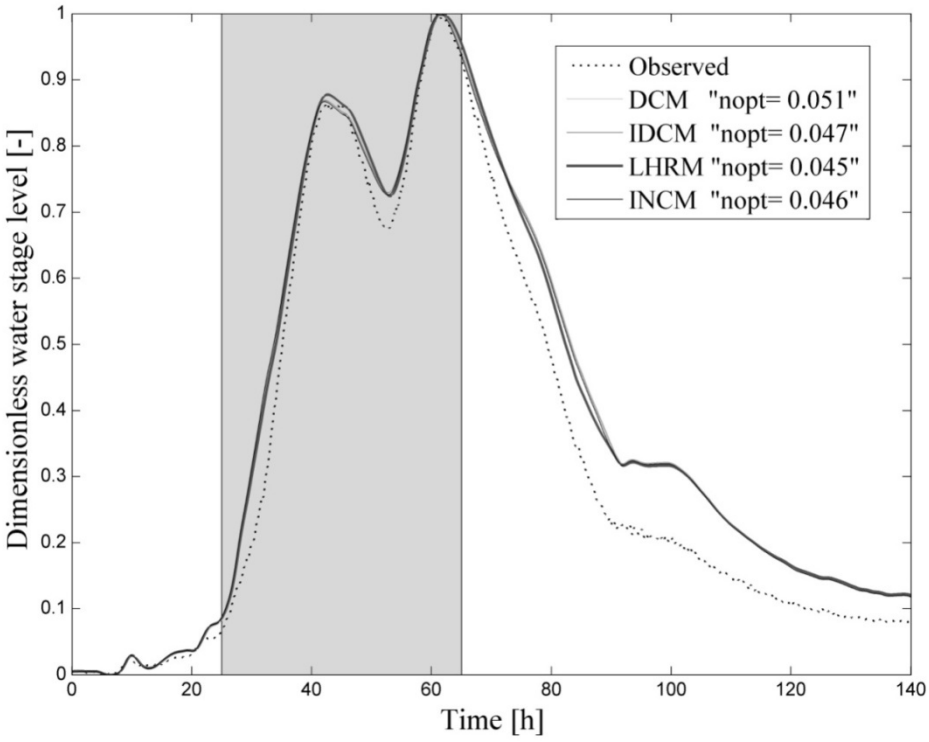

871

872 Figure 6 Observed and simulated stage hydrographs at Hunsdorf gauged site in the
873 event of January 2007.

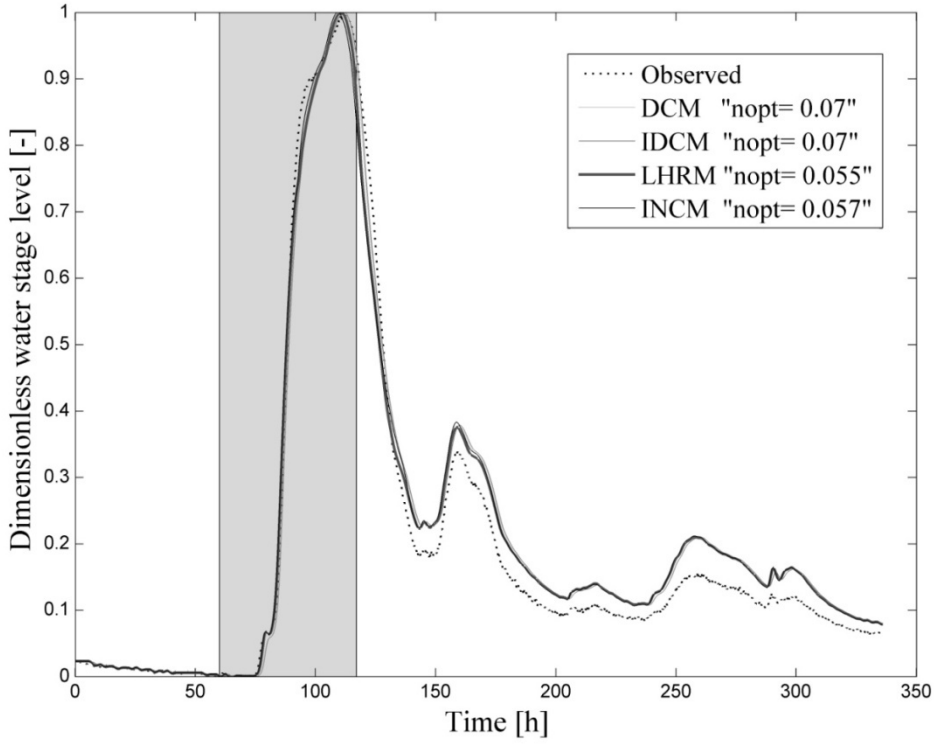

874

875 Figure 7 Observed and simulated stage hydrographs at Hunsdorf gauged site in the
876 event of January 2011.

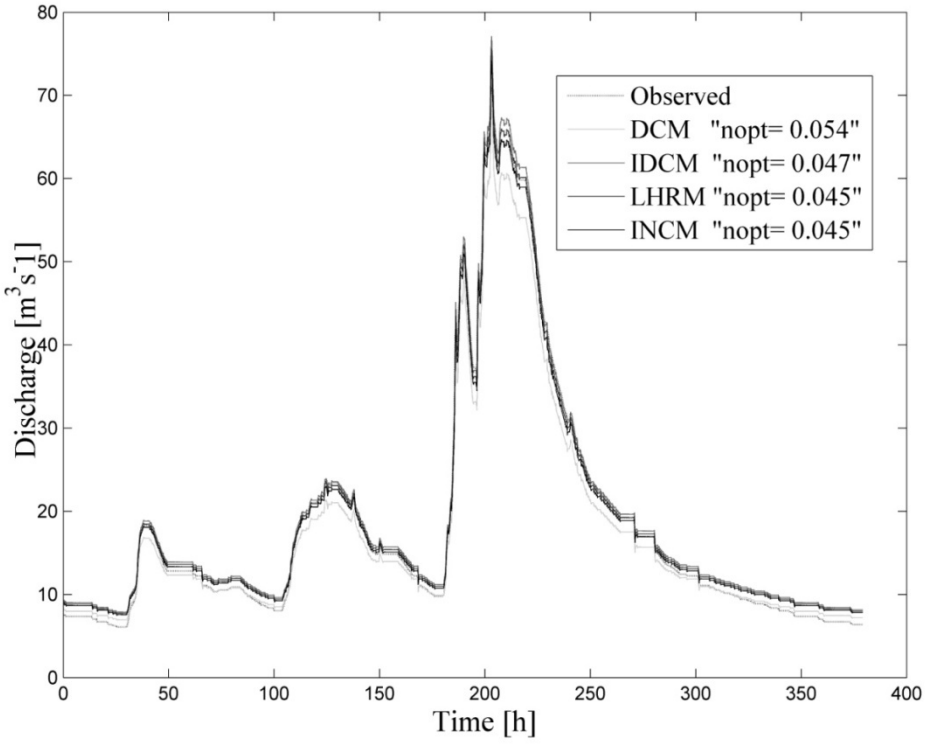

877

878 Figure 8 Observed and simulated discharge hydrographs at Pfaffenthal gauged site in
879 the event of January 2003.

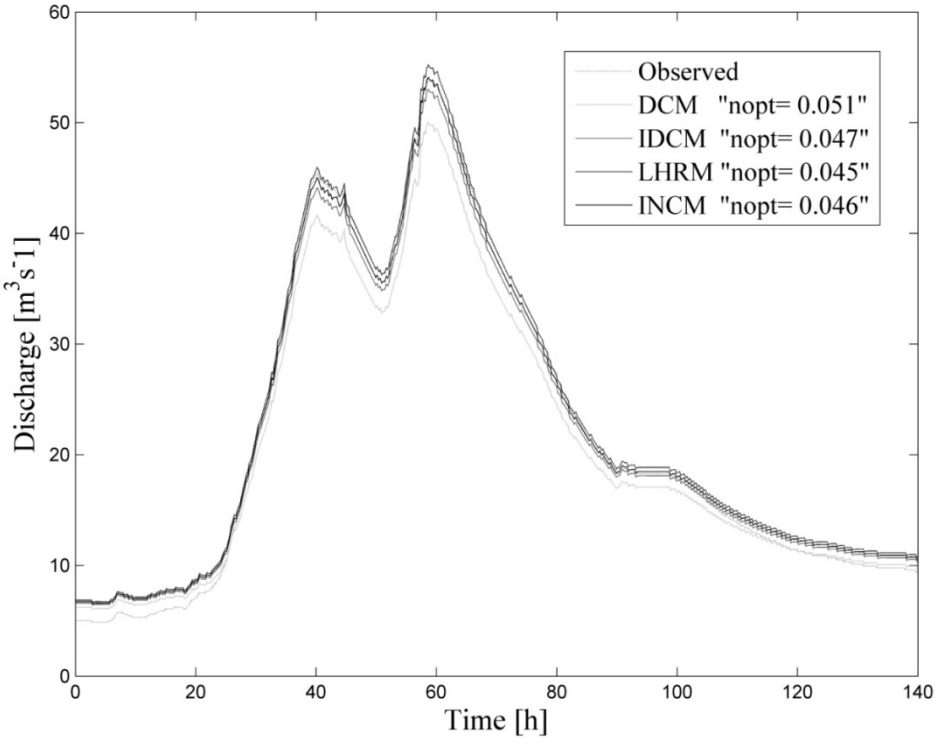

880

881 Figure 9 Observed and simulated discharge hydrographs at Pfaffenthal gauged site in
882 the event of January 2007.

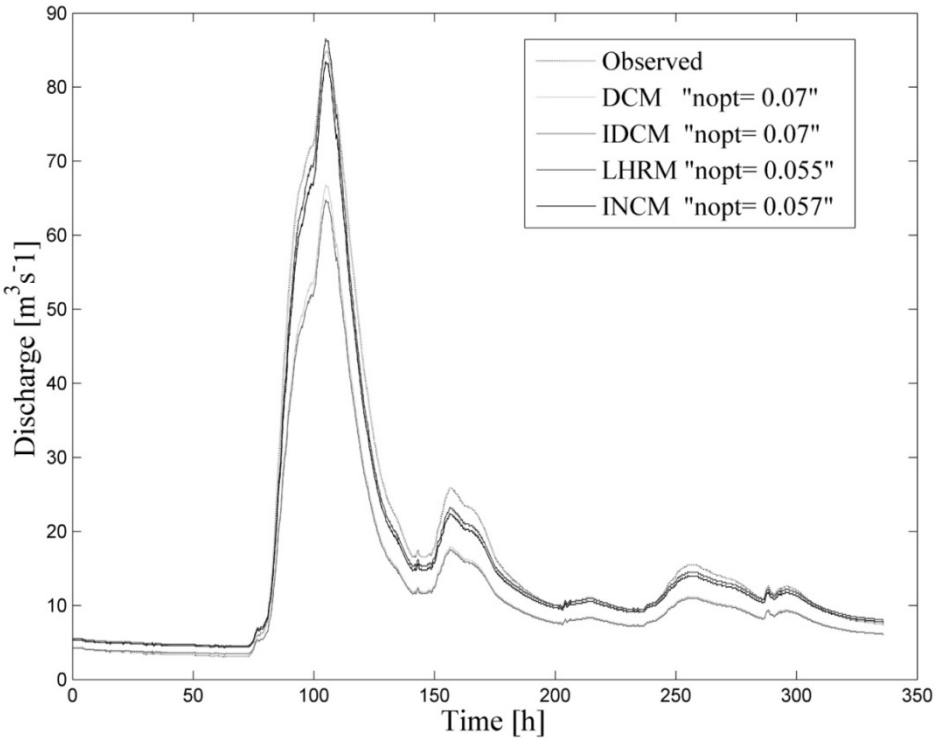

883

884 Figure 10 Observed and simulated discharge hydrographs at Pfaffenthal gauged site in
885 the event of January 2011.

886

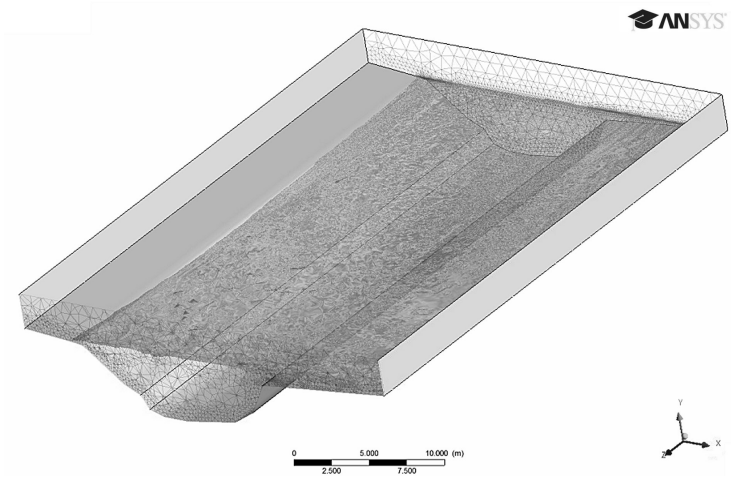

887

888 Figure 11 Computational domain of the reach of the Alzette river.

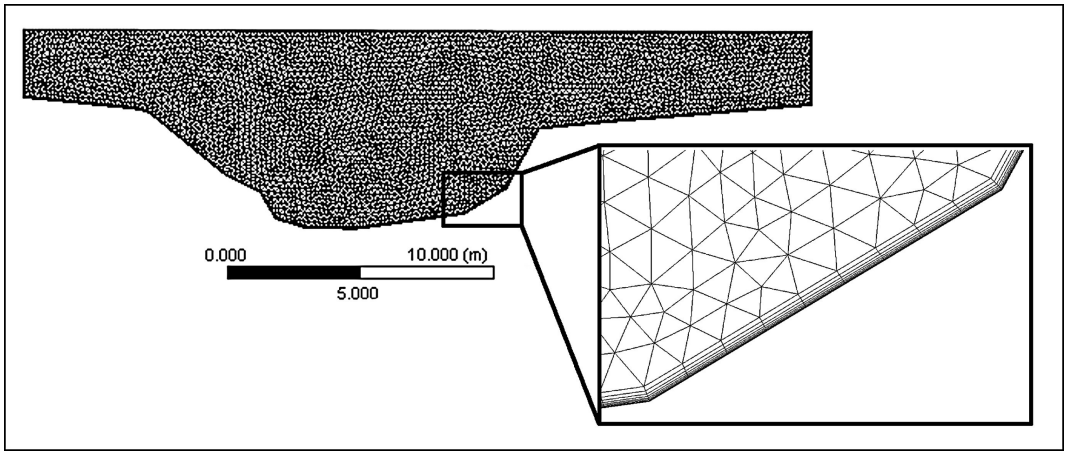

Figure 12 A mesh section along the inlet surface.

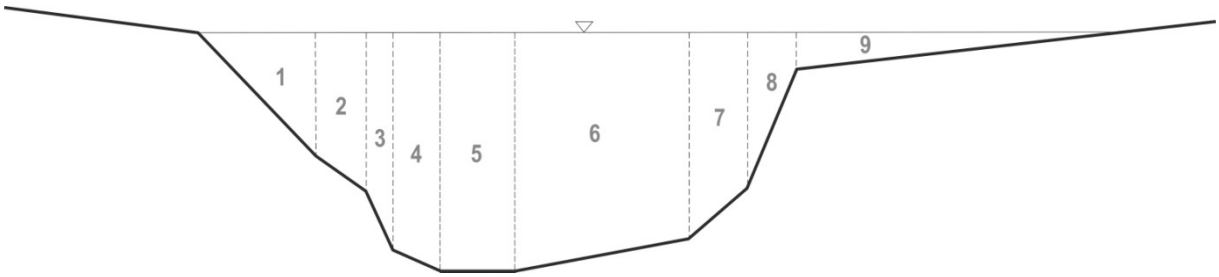

Figure 13 Hunsdorf river cross-section: subsections used to compute the vertically averaged velocities.

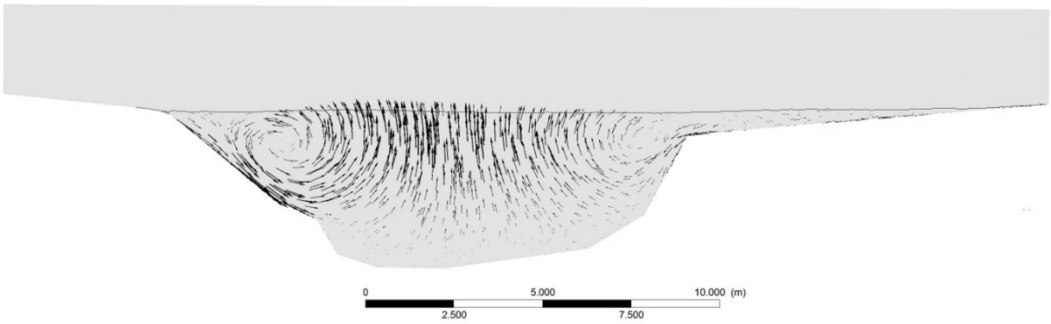

Figure 14 Secondary flow inside the intermediate cross section.

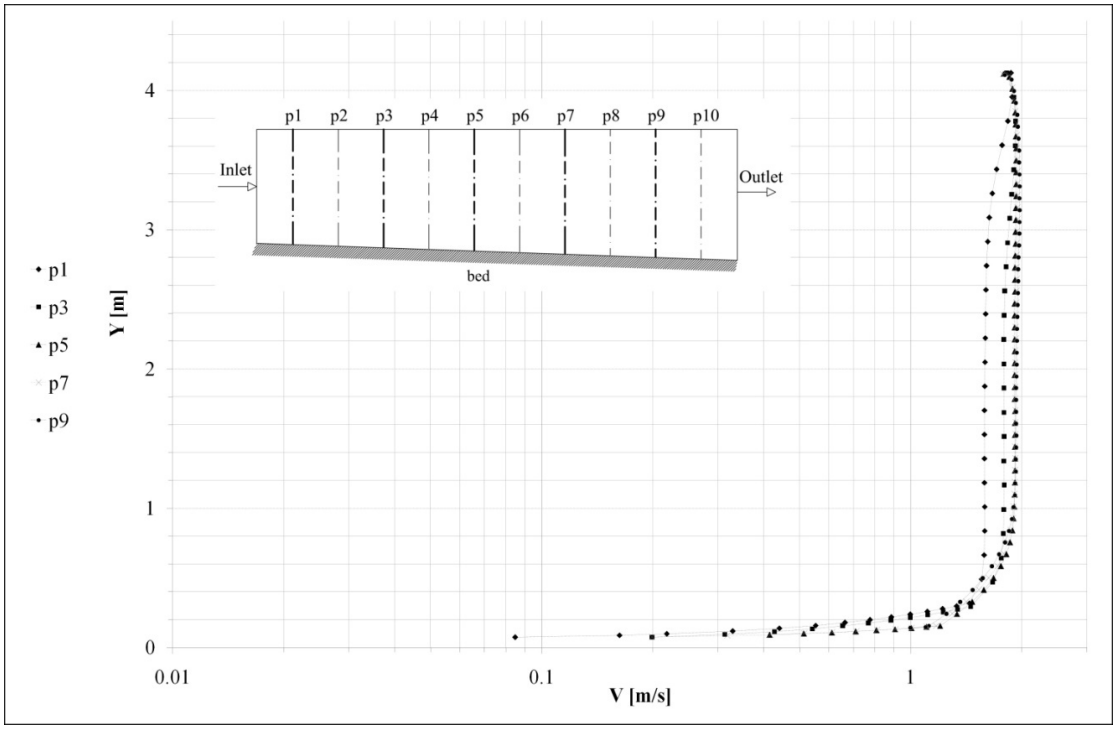

Figure 15 Streamwise vertical profile along the longitudinal axis of the mean channel.